HBRC Journal (2016) **12**, 163–174

Housing and Building National Research Center

HBRC Journal

http://ees.elsevier.com/hbrcj

Buckling strength of tapered bridge girders under combined shear and bending

Metwally Abu-Hamd [a], **Farah F. El Dib** [b,*]

[a] *Structural Engineering Dept., Cairo University, Egypt*
[b] *Steel Constructions Institute, HBRC, Giza, Egypt*

Received 21 September 2014; revised 19 October 2014; accepted 1 November 2014

KEYWORDS

Tapered plate girders;
Web buckling;
Combined shear and bend buckling;
Elastic stability

Abstract This paper represents the finite element results for the local buckling of tapered plate girders subjected to combine pure bending and shear stresses. An idealized model is developed representing the loading of the tapered panel that generates uniform normal stresses due to flexure, or uniform and constant shear stresses in the case of shear. Eigen-value analysis was performed for several tapered web plate girders that have different geometric parameters. A parametric study is made to reduce the FE model size showing the effect of decreasing the tapered panel adjacent straight panels, maintaining the same result accuracy as a complete girder model. The combined buckling capacity of bending and shear is determined by applying all possible load pattern combinations, together with different interaction ratios. An analysis study is presented to investigate the effect of the tapering angle on the combined bending–shear capacity of the girder. The study also includes the effect of the flange and web slenderness on the local buckling of the girder. Considering residual stresses as part of the loading stresses, the analysis procedure is repeated for some cases, and the effect of combining of the residual stresses together with the external loads is found. Empirical approximate formulae are given to estimate the combined flexure–shear buckling resistance of the tapered girder safely.

Introduction

Plate girders are widely used in steel structures, especially when there is a need to resist high loads, such as in bridges. The use of deep slender web girders is often chosen to give an adequate design. The tapering of the web depth can be implemented to avoid the use of excessive material quantities. Due to the web slenderness, the girder panel usually suffers instability due to the presence of normal and/or shear stresses. Normal stresses are usually induced due to flexural stresses, or due to the inclined component of shear stresses. For relatively short

* Corresponding author.
E-mail addresses: abuhamd@eng.cu.edu.eg (M. Abu-Hamd), farah_fayrouz@yahoo.com (F.F. El Dib).

Peer review under responsibility of Housing and Building National Research Center.

Production and hosting by Elsevier

http://dx.doi.org/10.1016/j.hbrcj.2014.11.001

panels, flexural stresses may cause compression buckling of the web or local buckling of compression flange. Shear stresses mainly cause shear buckling of the web.

Current design codes such as EN 1993-1-5 [1], AASHTO [2], are based on the theoretical and numerical research of prismatic girders, and they determine bending and/or shear resistance of tapered girders as prismatic ones.

This paper is divided into three parts. The first part demonstrates the finite element model, as well as the idealized loading model that is aimed at generating uniform flexural stresses without shear stresses, or vice versa. Hence, by applying both bending and shear patterns with different loading ratios and various direction combinations, the interaction bending–shear resistance is determined for loading ratios that express the accurate effect of bending and/or shear stresses on the elastic buckling strength of the tapered panel. The second part represents the analysis studies performed using the FEM Eigen-value analysis. Bending–shear interaction diagrams are plotted for different loading ratios, including several web and flange slenderness ratios, panel length ratios and tapering ratio. Furthermore, the obtained results investigate the effect of web tapering angle on the interaction capacity of the tapered plate girder.

Finally discussion and conclusions are given upon the performed analysis, and recommendations are given for future work.

Literature review and state of the art

Eid [3], presented the first known analysis of tapered thin plates using the finite difference method. He established numerical expressions for the inclined plate edges. He also solved the bending of plates under randomly distributed lateral loads, as well as buckling problems of tapered thin plates subjected to in plane acting loads. He compared the tapered thin plates with equivalent rectangular ones having the same critical load under different types of loading. He considered the effect of buckling shape and the number of half waves on the minimum critical buckling stresses.

Mirambell and Zarate [4], Estrada [5], and Chacon [6] presented a series of research papers concerning the elastic and inelastic ultimate strength for shear buckling of tapered web plate girders. Estrada [5] developed an expression to determine the critical shear buckling stress in steel web panels. This expression takes into account the effects of material nonlinearity together with the actual boundary conditions of the web panel.

Mirambell et al. [7–9], introduced an analytical formulation to determine the shear elastic buckling stress factor including the effect of flange slenderness and tapering angle. They also introduced an interaction formula for bending–shear interaction that depends on tension field theory. They considered that the ability to represent the ultimate shear resistance of the tapered girder for the given model depends on the fact that when the maximum shear resistance is reached, the bending moment in the largest cross section is null. Recently, Mirambell and Zarate [8] continued their research on the shear resistance of tapered web plate girders considering geometrical imperfections and residual stresses numerically, and comparing the results to experimental tests.

Abu-Hamd and Abu-Hamd [10] conducted full girder model demonstrating and determining the effect of flange slenderness on the pure flexural or pure shear elastic local buckling of a tapered panel. They were the first to introduce a model with a self-equilibrated loading pattern to achieve pure flexural or shear stresses in order to study each buckling case solely. The loading pattern developed in this paper depends on the same principal of equilibrating the loads such that the stresses are pure, but with the pattern configuration implemented to increase stress uniformity for either shear stresses or flexural normal stresses. They compared the results of pure bending and pure shear to the AASHTO [2] specifications. In addition, they conducted a parametric study and evaluated the buckling stress factors of pure shear and pure bending by varying the tapering ratio and web and/or flange slenderness. They recommended an investigation of the effect of combined shear and bending and post buckling behavior. Herein, the study aims at investigating the effect of combined shear and bending on the stability of tapered web plate girders, including geometrical parameters such as the web and flange slenderness, as well as, the tapering ratios.

Finite element analysis

Elastic buckling strength

The theoretical elastic buckling stress of a rectangular plate, σ_{cr}, is given by the widely known formula [11]:

$$\sigma_{cr} = k_{\sigma} \frac{\pi^2 E}{12(1-v^2)} \left(\frac{t}{d}\right)^2 \tag{1}$$

where E is the modulus of elasticity, v is Poisson's ratio, t is the thickness of the plate, d is the width of the plate, and k_{σ} is the plate buckling factor, which depends on the type of stress distribution and the edge support conditions.

Finite element analysis may be used effectively to obtain the elastic buckling stress under a wider scope of design variables related to the applied stresses and actual boundary conditions Earls [12], Ziemian [13], and Real et al. [14]. The buckling stress is obtained by solving the Eigen-value problem:

$$K_E = \lambda K_G \tag{2}$$

where K_E is the elastic stiffness matrix, K_G is the geometric stiffness matrix, and λ is the Eigen-value, which represents the buckling load factor. The corresponding Eigen-vector represents the mode shapes of the buckled plate.

Idealized loading of the model

The plate buckling solution initiated by Timoshinko [11] is based on homogeneous and pure stresses, normal or shear, in one or two directions, and acting in the middle plane. Later different code provisions adopted simplified interaction analyses between different stress cases to simplify the design approach. Abu-Hamd and Abu-Hamd [10] presented idealized load patterns providing pure normal or shear stresses and calculated accurate basic buckling analysis for either shear or bending.

They found that interaction-buckling analysis is very sensitive and requires accurate models.

The given idealized loading in Abu-Hamd and Abu-Hamd [10] is further improved to achieve acceptable interaction accuracy for the large amount of cases expected. The accuracy of the proposed idealized loading is assured as follows:

- The loading pattern should apply close to the tapered web.
- The structural model size should be minimized.
- The loading should be distributed along the tapered web circumference to allow best pure distribution.
- The idealized loading distribution should comply with the web height variation.
- The idealized loading should be perfectly balanced [10].
- The idealized balanced loading should be valid and accurate as well, when reversed.

In order to study the effect of homogenous pure bending stresses and/or pure shear stresses on the buckling resistance of a tapered plate girder, two loading patterns are developed. Two patterns were delivered to generate either pure shear stresses or pure bending stress distribution on the tapered web panel of plate girder.

Initial loading pattern for pure shear

As shown in Fig. 1, at the start of numerical iteration, the panel is loaded at both ends with Shear Loads distributed along the web edges such that:

$$Q_1 = H_1 \cdot t_w \cdot \frac{F_y}{\sqrt{3}} \tag{3}$$

$$Q_2 = H_2 \cdot t_w \cdot \frac{F_y}{\sqrt{3}} \tag{4}$$

where Q_1 and Q_2 are the web shear forces of the web larger and lower depths, (H_1) and (H_2) , respectively. t_w is the web thickness. F_y is the yielding stress.

However, since Q_1 is larger than Q_2, a balancing vertical load (q_v) equal to the difference between their values is distributed along the upper and lower edges of the web panel such that:

$$q_v = \frac{(Q_2 - Q_1)}{2 \cdot \alpha \cdot H_1} \tag{5}$$

where α is the tapered panel aspect ratio.

So far the given loads are force equilibrated only. In order to establish rotation equilibrium, a horizontal balancing load (q_h) is distributed along the upper and lower edges of the web panel, the relation between this load and the other forces can be deducted using moment equilibrium condition around point (A), hence (q_v) vanishes, and the total horizontal load per unit length is:

$$q_h = \frac{2(Q_1 + Q_2)(\alpha H_1/2)}{(H_1 + H_2)\alpha H_1} = \frac{(Q_1 + Q_2)}{H_1 + H_2} \tag{6}$$

Initial loading pattern for pure moment

As shown in Fig. 2, the panel is loaded at both ends with pure moment loads (M_1 and M_2) that are distributed on the web edges and flange edges according to the following criteria:

$$M_1 = F_y t_w H_1^2/6 + P_{fy} \cdot H_1 \tag{7}$$

$$M_2 = F_y t_w H_2^2/6 + P_{fy} \cdot H_2 \tag{8}$$

where P_{fy} is the flange yielding force defined as following:

$$P_{yf} = B_f \cdot t_f \cdot F_y \tag{9}$$

where B_f and t_f are flange width and thickness, respectively.

Web moment stresses are applied on the vertical web ends in a triangular distributed pattern on the web nodes such that each stress on the web, (f_{1wi} or f_{2wi}), is given as follows:

$$f_{1wi} = \frac{2F_y \cdot h_{1i}}{H_1} \tag{10}$$

$$f_{2wi} = \frac{2.F_y \cdot h_{2i}}{H_2} \tag{11}$$

where (h_{1i}) and (h_{2i}) are the vertical distances between the panel web node and the section centerline, for the larger section and smaller section, respectively.

However, since M_{w1} is larger than M_{w2}, balancing stress (f_h) and force (P_{fy}) are applied to the model to balance the web moments (M_{w1}) and (M_{w2}) and the moment that results from the lower flange ends eccentricity due to web tapering, where balancing force (f_h) is distributed along the upper and lower flange directions such that:

$$f_h = \frac{2 \cdot (M_{w1} - M_{w2})}{\alpha \cdot H_1 \cdot t_w (H_1 + H_2)} \tag{12}$$

The relation, between the balancing force (P_v) and the moment that resulted from the lower flange end eccentricity, can be deducted using a moment equilibrium condition, so that:

$$P_v = \frac{P_{yf} \cdot (\phi \cdot H_1)}{(\alpha \cdot H_1)} = \frac{P_{yf} \cdot \phi}{\alpha} \tag{13}$$

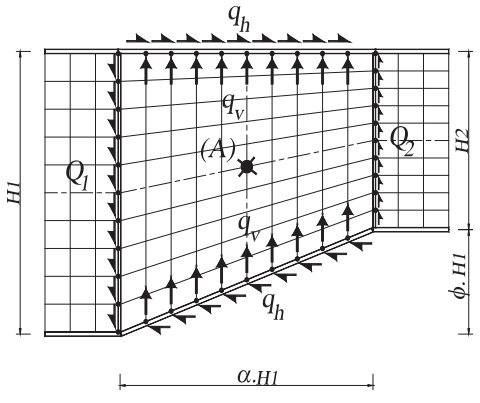

Fig. 1 Loading pattern for pure shear.

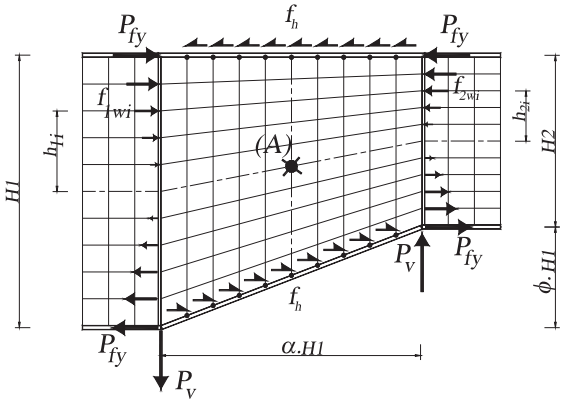

Fig. 2 Loading pattern for pure moment.

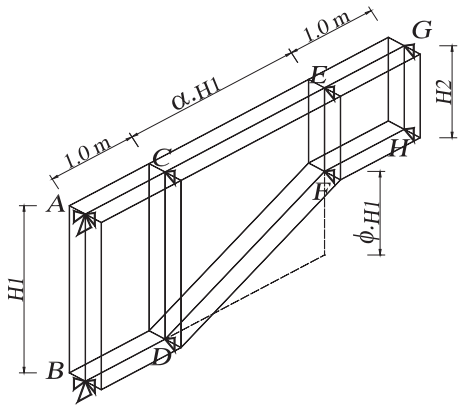

Fig. 3 Tapered girder model.

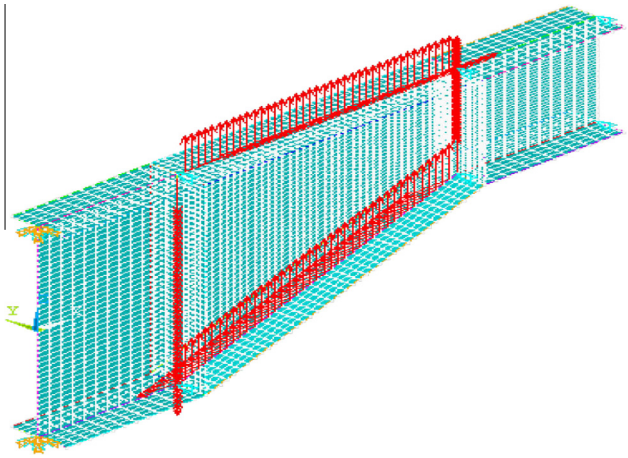

Fig. 4 Finite element model with shear loading.

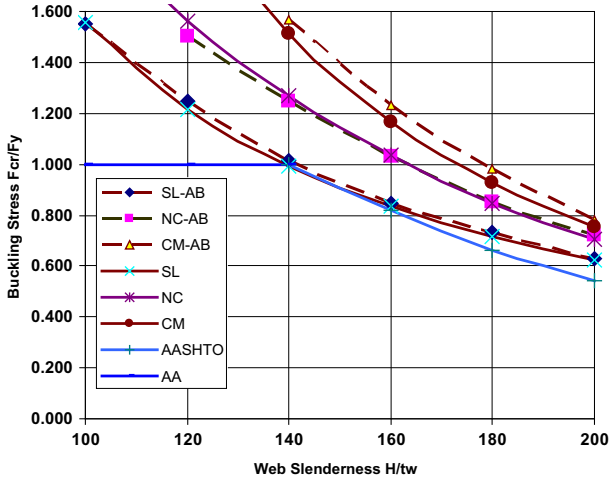

Fig. 5 Comparison to the results given in Abu-Hamd and Abu-Hamd [10].

where ϕ is the tapering ratio, that is the ratio between the difference of the larger and lower depths to the larger web depth, as shown in Figs. 1 and 2.

Hence, all the applied loads for each pattern are in equilibrium, and the stress uniformity is validated for each case to be constant shear stresses all over the tapered panel without bending for the shear loading pattern, or uniform normal flexural stresses without shear stresses for the moment loading pattern.

Table 1 F_{cr}/F_y for different model dimensions.

L_3/L_2 (ms)	$\lambda = 140$ $\phi = 0.5$ $\alpha = 1$	$\lambda = 140$ $\phi = 0.25$ $\alpha = 2$	$\lambda = 200$ $\phi = 0.5$ $\alpha = 1$	$\lambda = 200$ $\phi = 0.25$ $\alpha = 1$	$\lambda = 200$ $\phi = 0.25$ $\alpha = 2$
4.0/4.0	1.174	0.870	0.737	0.601	0.512
3.0/3.0	1.175	0.871	0.737	0.601	0.512
2.0/4.0	1.177	0.872	0.738	0.602	0.513
2.0/1.0	1.177	0.872	0.738	0.602	0.513
1.0/0.5	1.181	0.875	0.743	0.604	0.513

Table 2 Comparison to the results given in [9].

Model dimensions (mm)	Load	V_{cr} (kN)	V_{cr} (kN), num [9]	V_{cr} (kN), test [9]
A: 600 800 800 3.9 180 15	Q	237.8	223.9	225.0
B: 500 800 1200 3.9 180 15	Q	218.5	212.0	220.0
C: 480 800 800 3.9 180 15	Q	284.2	269.1	265.0
D: 600 800 800 3.9 180 15	M + Q	238.3	236.6	225.0

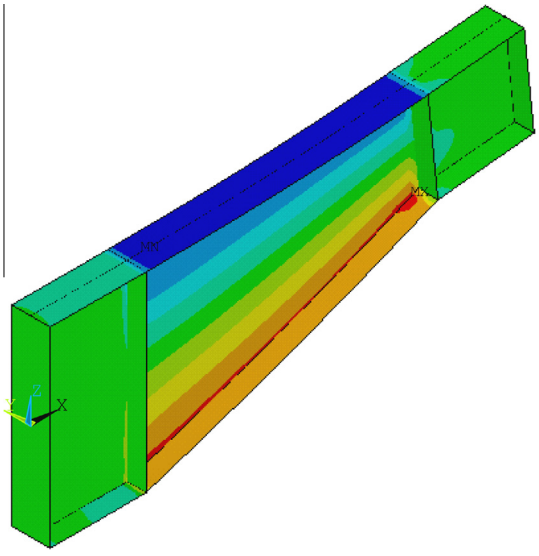

Fig. 6 Pure flexural stresses for moment pattern.

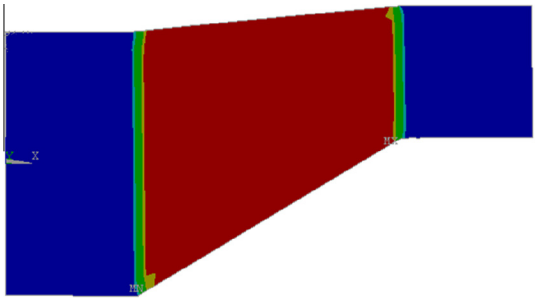

Fig. 7 Pure shear stresses for shear pattern.

Description of the idealized model

Fig. 3 shows the geometric configuration and dimensions, in addition to boundary conditions, of the tapered girder used in the study. The girder consists of three segments, and the middle one is the tapered panel under consideration. The straight segments each have a length of 1.0 m. The tapered segment length varies from 2 to 4 m to give variable aspect ratios (α) of 1 and 2. The deeper end web depth is taken equal to 2 m while the smaller end depth is varied from 1 m to 2 m at intervals of 0.25 m to give different tapering ratios (ϕ) of 0.125, 0.25, 0.375 and 0.5. The flange width is kept constant at 0.4 m or 0.5 m.

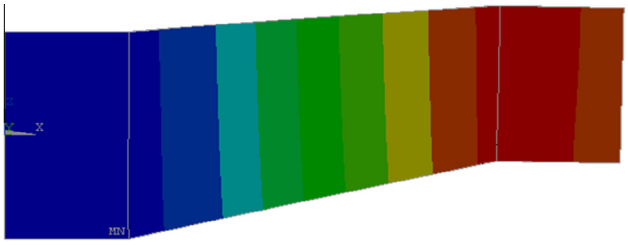

Fig. 8 Shear deformations.

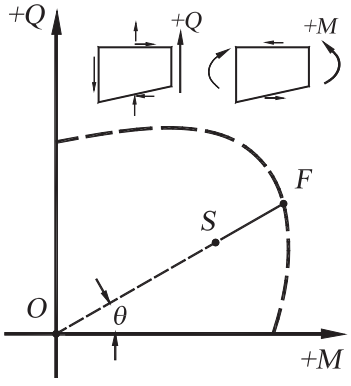

Fig. 9 Polar coordinates of combined load.

The two points (A) and (B), including their rigid stiffener, are restrained for displacement in all directions, while the rest of the points from (C) to (H) are restrained only for the out-of-plane displacement as shown in Fig. 3.

Finite element model

Fig. 4 shows the finite element model representing the model girder. All plate elements are modeled with an iso-parametric finite strain shell element designated as "Shell 181" in the ANSYS [15] element library. Shell 181 is a four-noded shell element with six degrees of freedom per node and has geometric and material nonlinearity capabilities. It is well suited for linear, large rotation, and/or large strain nonlinear applications. In the construction of the finite element model, convergence was achieved by using an element size of 40–60 mms. Lateral-torsional buckling was prevented, as the flange out-of-plane stiffness was adequate to restrain the panel against this phenomenon. The material properties used are Elastic modulus $E = 210$ GPa, yield stress $F_y = 350$ MPa, and Poisson's ratio $v = 0.3$. The number of models established and presented in this study is 546 models including variance in parameters such as flange slenderness, web slenderness and moment-shear variable load pattern ratios.

Validation of the finite element model

In order to check the accuracy of the finite element solution procedure a comparison is made with the pure bending results given in Abu-Hamd and Abu-Hamd [10]. The selected parameters for comparison are aspect ratio (α) of 1.0, and tapering ratio (ϕ) of 0.25, using a tapered panel largest depth of 2.0 m. The variation of the buckling stress was compared at different web slenderness ratios (H/t_w) for: compact flange (CF), non-compact flange (NCF), and slender flange (SF) as shown in Fig. 5.

The effect of adjacent straight panels is maintained by reducing their lengths through a parameter variation. This effect was almost negligible (Table 1).

Furthermore, the results of the currently used model showed good agreement with the results of the previous study,

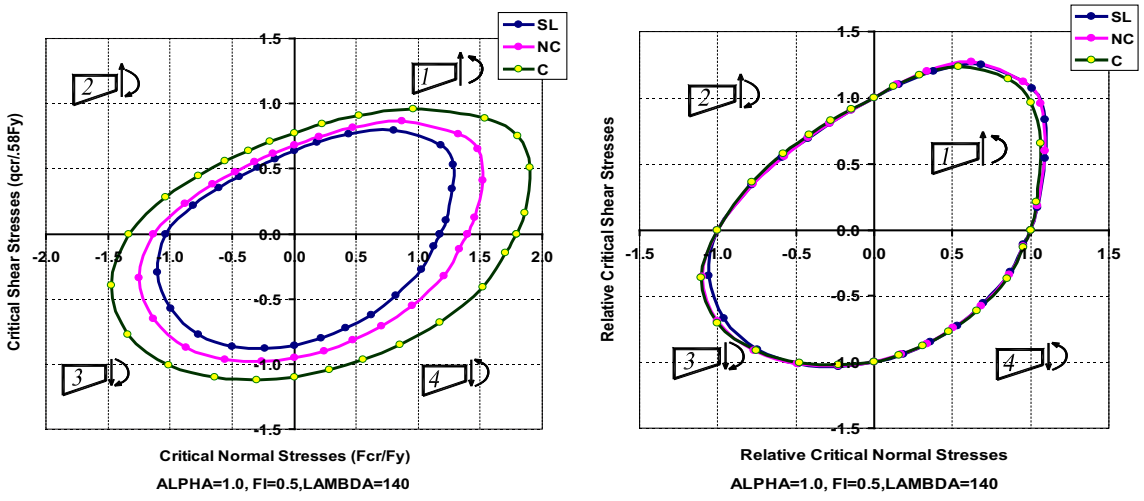

Fig. 10 Stresses and relative interaction ($\lambda = 140$, $\alpha = 1$, $\phi = 0.5$).

which proves that the model of the current study is representing the behavior of the tapered panel as the complete girder model does.

Another model is compared to the results given in the extensive numerical and testing research of Mirambell and Zarate [4], and is considered as half of its almost symmetric model. The comparison of results is given in Table 2:

For Table 2, the mentioned dimensions are the shorter depth, the larger depth, the panel length, the web thickness, the flange width and the flange/stiffener thickness respectively.

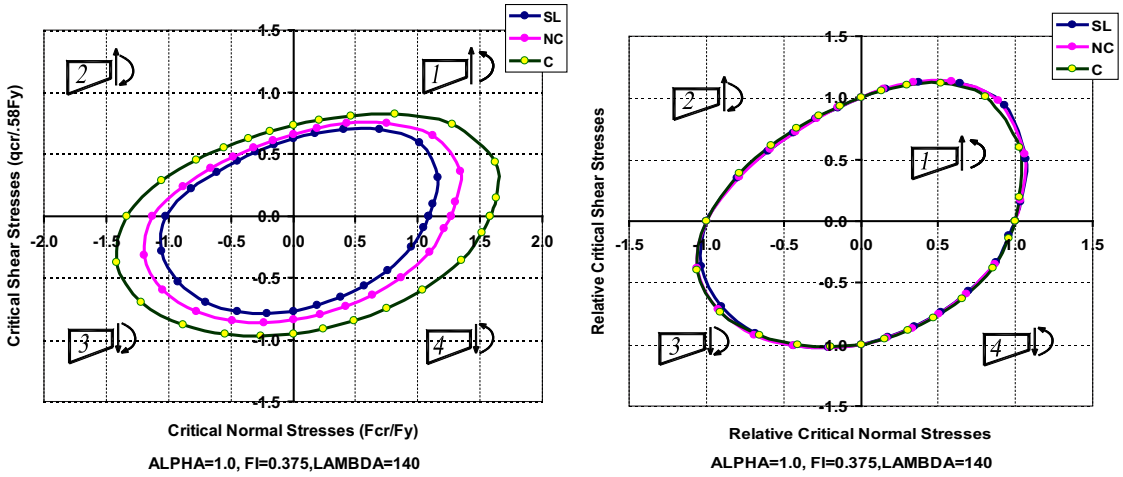

Fig. 11 Stresses and relative interaction ($\lambda = 140$, $\alpha = 1$, $\phi = 0.375$).

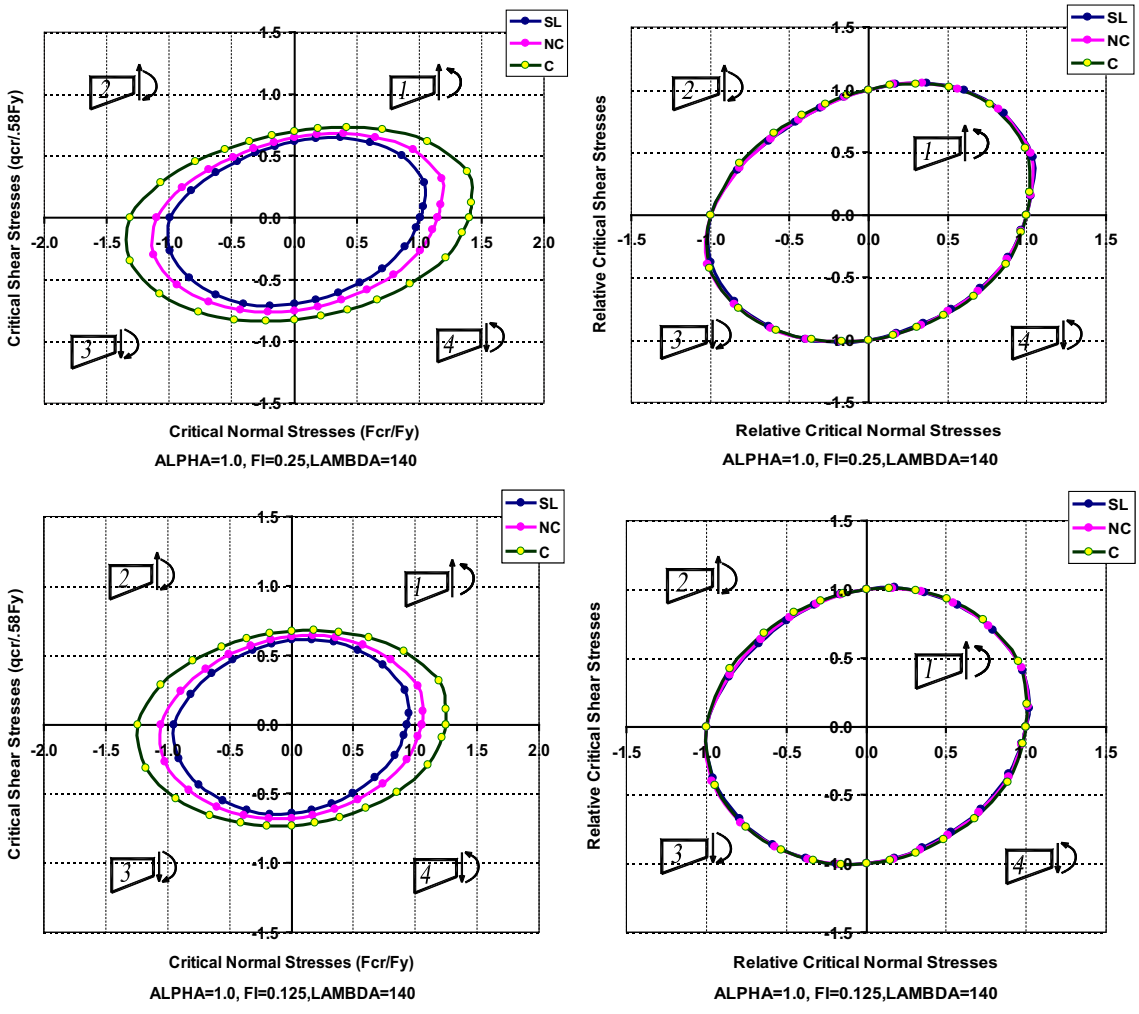

Fig. 12 Stresses and relative interaction ($\lambda = 140$, $\alpha = 1$, $\phi = 0.25, 0.125$).

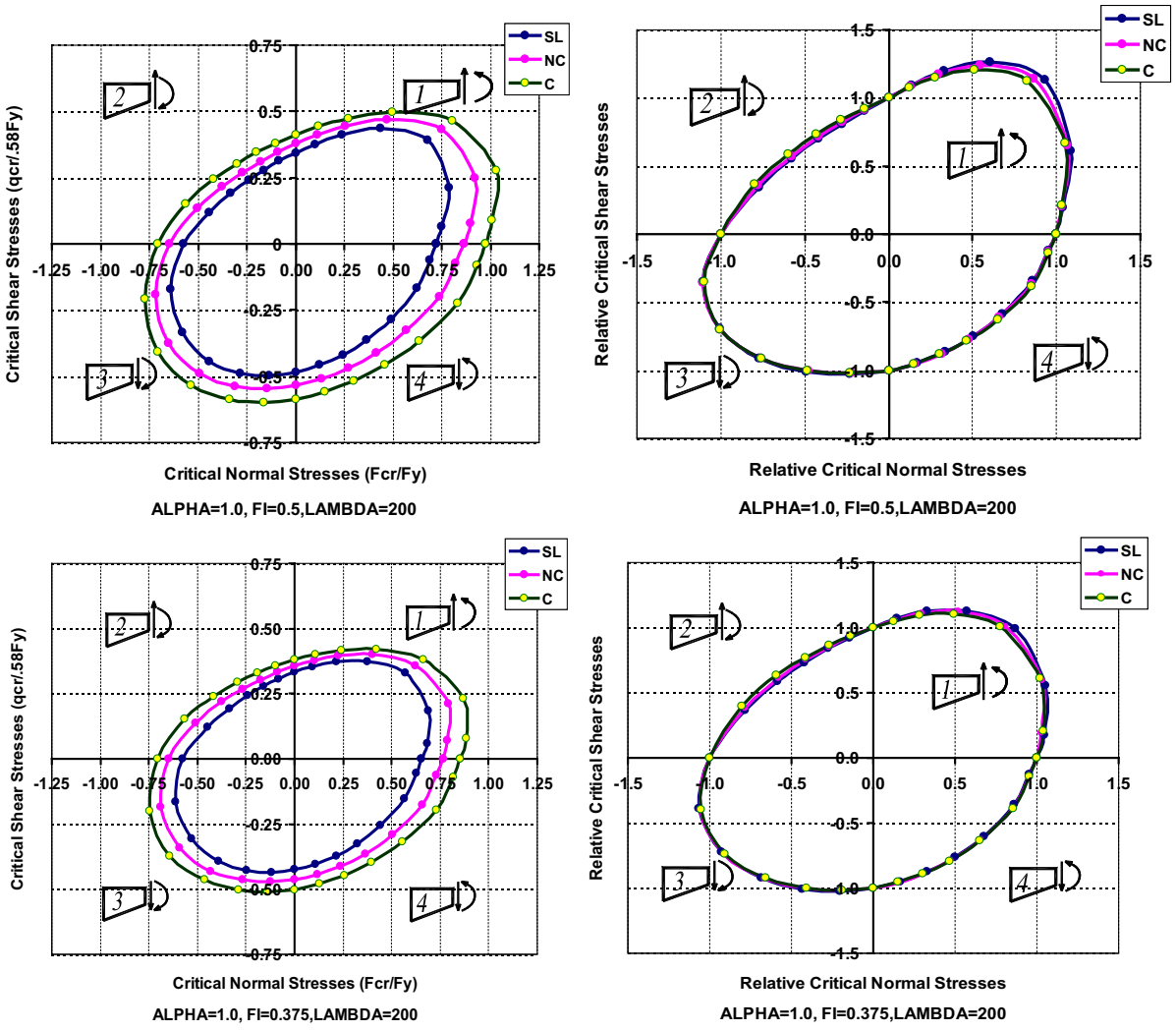

Fig. 13 Stresses and relative interaction ($\lambda = 200$, $\alpha = 1$, $\phi = 0.5, 0.375$).

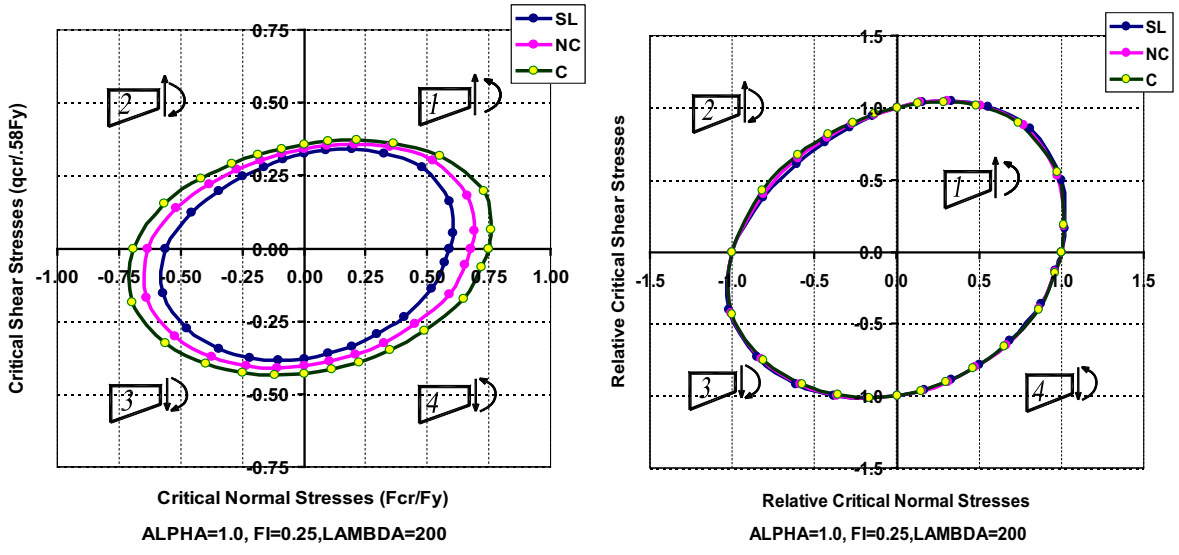

Fig. 14 Stresses and relative interaction ($\lambda = 200$, $\alpha = 1$, $\phi = 0.25$).

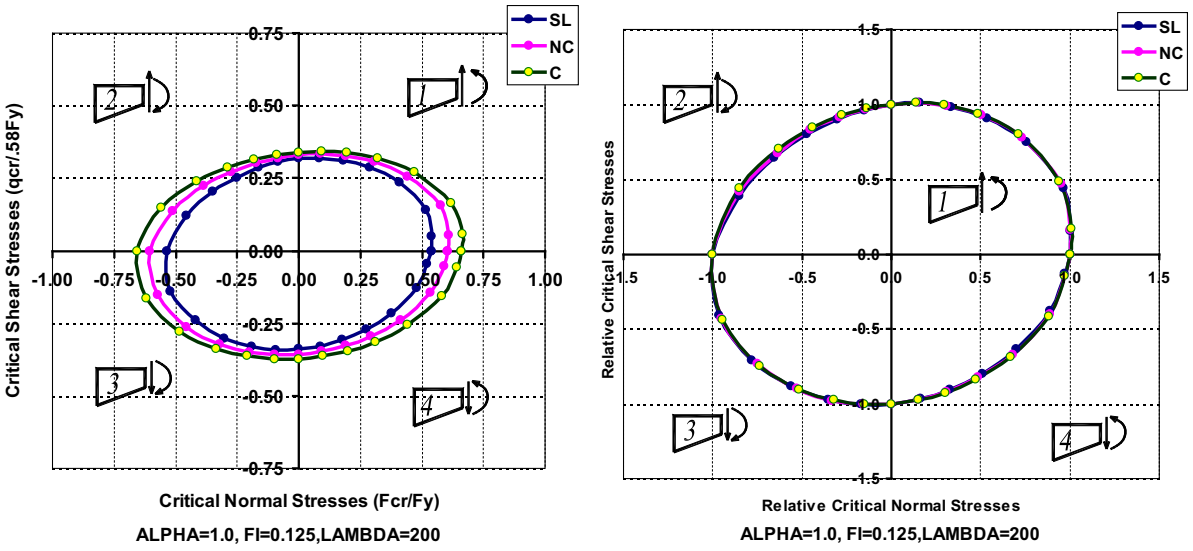

Fig. 15 Stresses and relative interaction ($\lambda = 200$, $\alpha = 1$, $\phi = 0.125$).

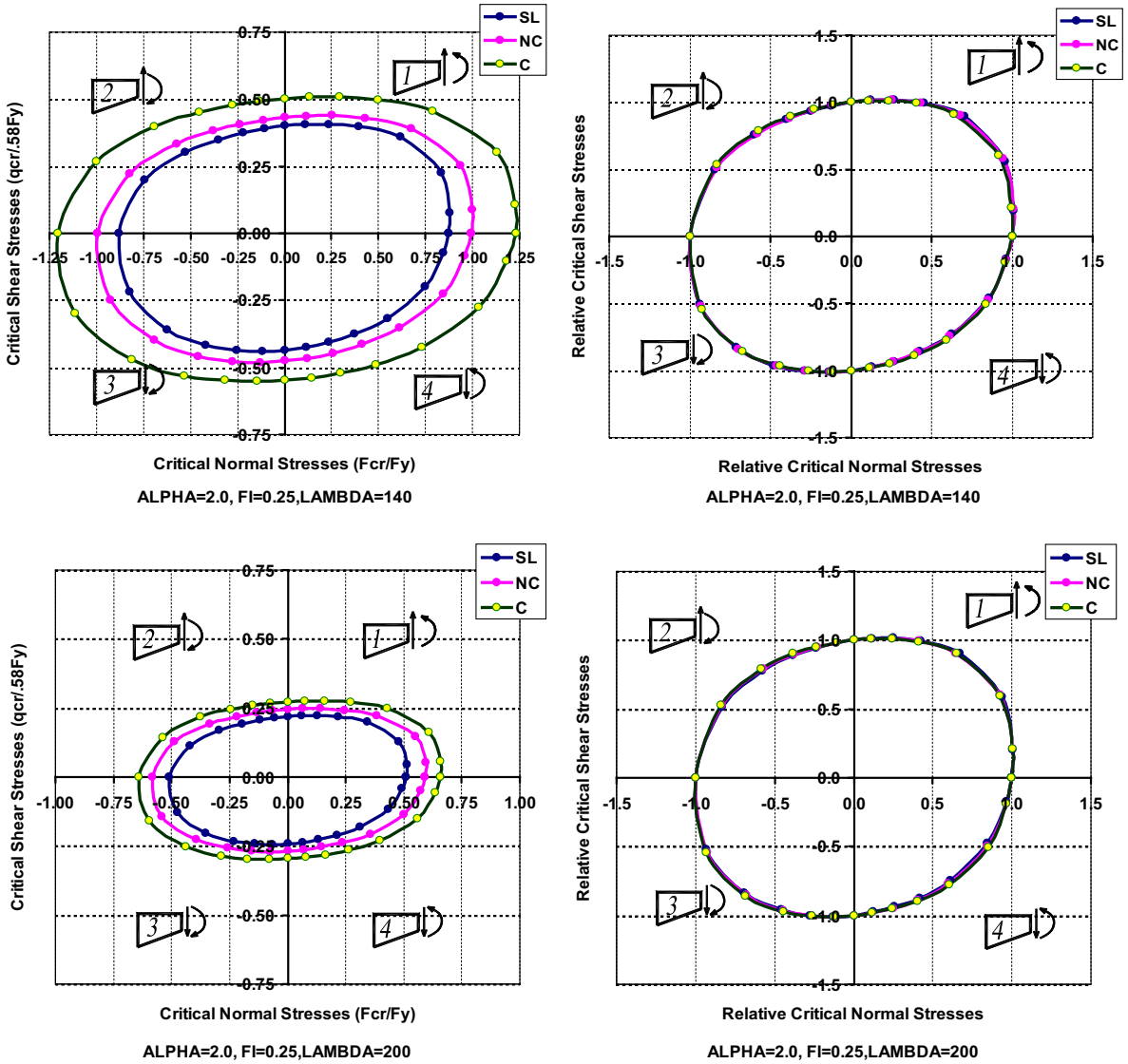

Fig. 16 Stresses and relative interaction ($\lambda = 140{,}200$, $\alpha = 2$, $\phi = 0.25$).

Considering the differences between the models, the accuracy is acceptable.

Analysis and results

Accuracy of the numerical model

Applying the idealized loading on an evaluation sample case, a pure stress and uniform deformation patterns are found for either bending stresses or shear stresses, as illustrated in Figs. 6–8. Fig. 6 shows the variation of the normal stress resulting from the case of pure flexure; the normal stresses along the upper and lower flanges indicate the validity of the assumptions of the finite element loading model.

We note in Fig. 7 that the stress color border falls on the input shear stress value of $F_y/\sqrt{3}$ with minor variation in shear stresses of about 0.5% in both directions. The minor variations are due to corner concentrations, and do not affect the uniformity of the web stress.

Presentation and analysis of the results

Fig. 9 sketches the used polar determination of the Eigen-value of the buckling interaction of moment and shear. It starts with a stress vector OS and θ. The analysis outputs the multiplier of the final result that equals OF/OS. The bending and corresponding shear results are then (OF $\cos\theta$) and (OF $\sin\theta$) respectively. The forces shown in Fig. 9 are the respective resultants of the web edge model stresses. A logo is placed on the result plot sketch to indicate the type of combination as described in Section 'Approximate direct solution'.

The starting stress values (F_{start}) are either F_y or 0.58 F_y in cases of pure moment or pure shear respectively. By selecting the starting fractions in polar coordinates, with the radius equal to unity and taking the angle "θ", as a variable, thus the starting stresses are:

$$F_{start,M} = F_y \cdot \cos\ \theta \tag{14}$$

$$F_{start,Q} = \frac{F_y}{\sqrt{3}} \sin\ \theta = 0.58F_y \cdot \sin\ \theta \tag{15}$$

The buckling multiplier β_{cr}, resulting from the buckling analysis, is the buckling ratio of the mixed loading as a whole, and should then be multiplied to each of the above two values to finally determine the two critical buckling stresses ($F_{cr,M}$) and ($F_{cr,Q}$) of one interaction case. Two different methods to plot the results are used: the interaction critical stress values and the relative interaction relationship: which is related to each of the critical values of pure stresses starting and ending the relationship at unity. The corresponding parameters are given on each plot, where:

$$\frac{F_{cr,M}}{F_y} = \beta_{cr} \cdot \cos\ \theta \tag{16}$$

$$\frac{F_{cr,Q}}{0.58F_y} = \beta_{cr} \cdot \sin\ \theta \tag{17}$$

By varying θ from 0 to 360°, all results, before or beyond 1.0, can be captured, and all kinds of direction combinations between the combined moment and shear can be considered. The results of tapered web buckling behavior, under all load typologies, are displayed by the critical values, from Figs. 10–16.

Approximate direct solution

It is easier and safe to use the following approximate formulae to estimate the relative buckling stresses of combined bending and shear, where Type 1 load orientation is shown in Figs. 1 and 2. Type 2 load orientation is shown in Fig. 1 and reversed Fig. 2. Type 3 load orientation is the reverse of what is shown in Figs. 1 and 2. And finally Type 4 load orientation is shown in Fig. 2 and reversed Fig. 1.

For Types (1) and (3)

$$\left(\frac{M_i}{M_{cr}}\right)^A + \left(\frac{Q_i}{Q_{cr}}\right)^A = 1 \tag{18}$$

where M_i and Q_i are the relative interaction bending and shear stresses, and

$$A = \left(1.9 + 4\frac{\phi}{\alpha}\right) \tag{19}$$

The increase in shear resistance due to moment characterizes these two types, as indicated in Figs. 10 and 13. Fig. 17 demonstrates this phenomenon.

For Types (2) and (4)

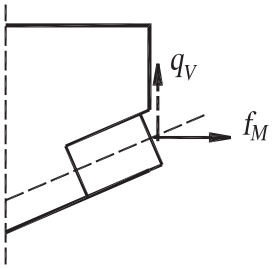

Fig. 17 Tapering element stress analysis.

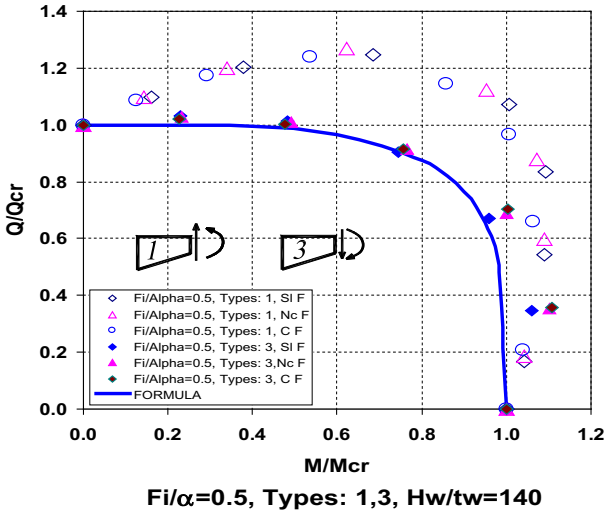

Fig. 18 Comparison between approximate and accurate analysis (ϕ/α = 0.5, Types 1 and 3, H_w/t_w = 140, α = 1.0).

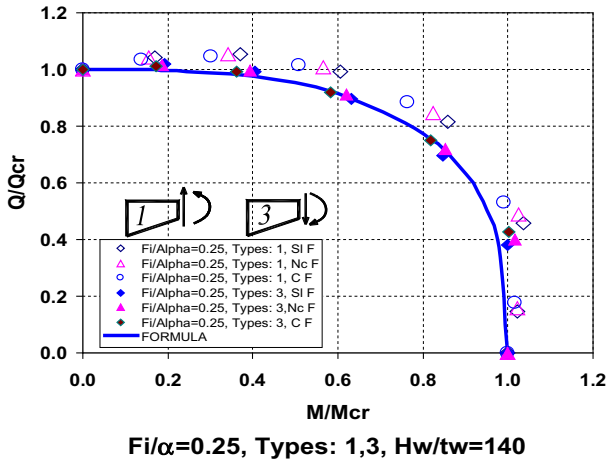

Fig. 19 Comparison between approximate and accurate analysis ($\phi/\alpha = 0.25$, Types 1 and 3, $H_w/t_w = 140$, $\alpha = 1.0$).

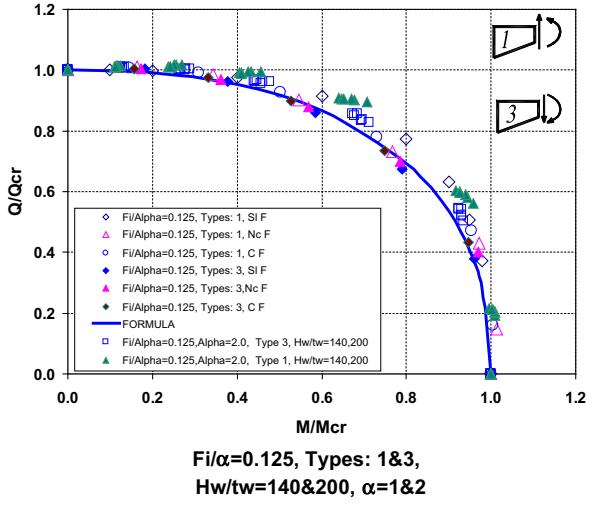

Fig. 20 Comparison between approximate and accurate analysis ($\phi/\alpha = 0.125$, Types 1 and 3, $H_w/t_w = 140$ and 200, $\alpha = 1$ and 2).

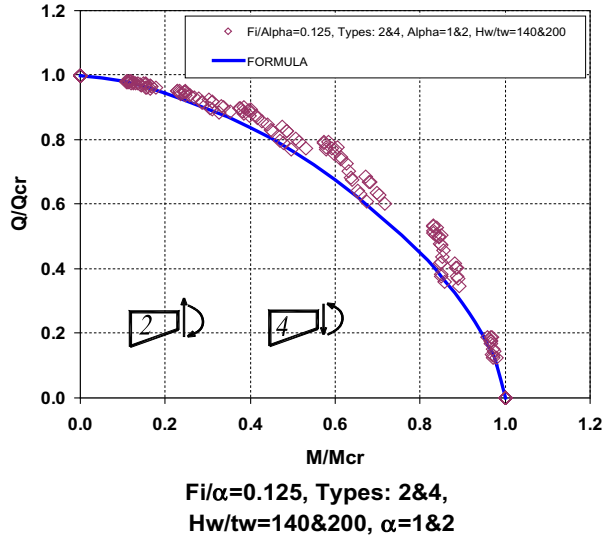

Fig. 21 Comparison between approximate and accurate analysis ($\phi/\alpha = 0.125$, Types 2 and 4, $H_w/t_w = 140$ and 200, $\alpha = 1$ and 2).

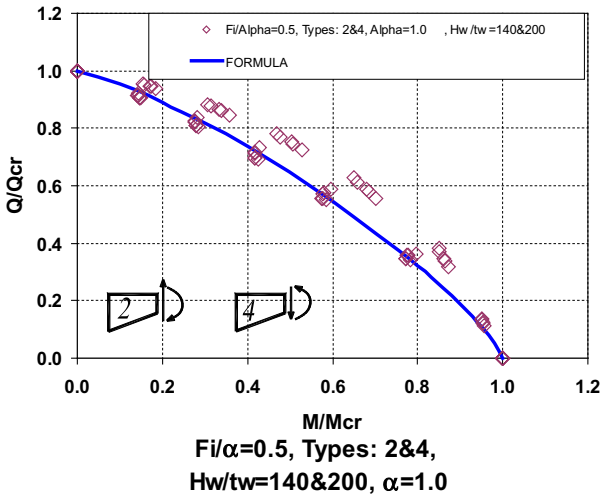

Fig. 22 Comparison between approximate and accurate analysis ($\phi/\alpha = 0.5$, Types 2 and 4, $H_w/t_w = 140$ and 200, $\alpha = 1$).

$$\left(\frac{M_i}{M_{cr}}\right)^B + \left(\frac{Q_i}{Q_{cr}}\right)^B = 1 \tag{20}$$

where M_i and Q_i are the relative interaction bending and shear stresses, and

$$\mathrm{B} = \left(1.9 - \sqrt{\frac{\phi}{\alpha}}\right) \tag{21}$$

These two types suffer a reduced shear resistance due to moments.

The accuracy of the approximate formulae is given in Figs. 18–22, noting that in Fig. 18 no use could be made above a relative value of 1.0 because it gives double results and the least one must be taken: (For example: a relative $Q = 1.08$ gets relative $M = 0.16$ or 1.07). In the above equations: α is the aspect ratio and ϕ is the tapering ratio (Fig. 3).

Effect of residual stresses

By assuming the residual stresses as "Element Loads", the values of these stresses are included in the "Element Stiffness

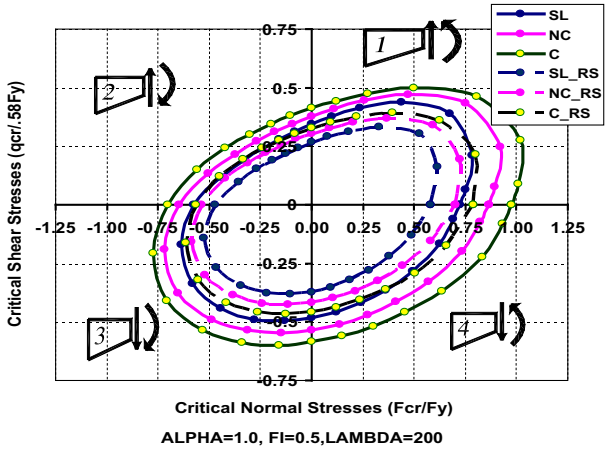

Fig. 23 Comparison between Stress Interaction with and without residual stresses ($\alpha = 1.0$, $\phi = 0.5$, $\lambda = 200$).

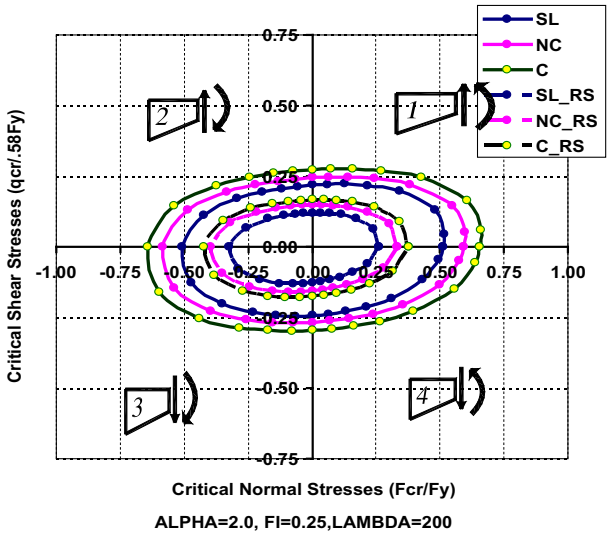

Fig. 24 Comparison between stress interaction with and without residual stresses ($\alpha = 2.0$, $\phi = 0.25$, $\lambda = 200$).

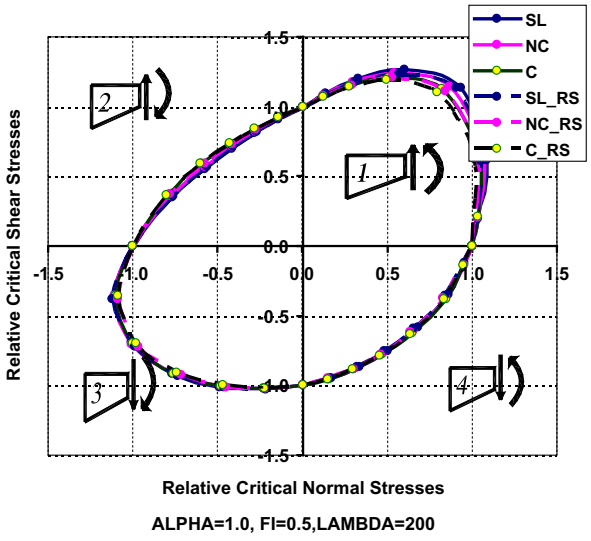

Fig. 25 Comparison between relative interaction with- and without residual stresses ($\alpha = 1.0$, $\phi = 0.5$, $\lambda = 200$).

Matrix" and the resulting Eigen-values shall change. By applying the analysis on the following examples, we can estimate such influence on the interaction between shear and bending stresses. The example covers the following parameters: $\alpha = 1.0$, $\phi = 0.5$ and 0.25, for Lambda $= H_w/t_w = 200$. By inspecting Figs. 23 and 24, we notice a clear reduction in the critical shear and moment stresses. Nevertheless, Figs. 25 and 26 show values that are almost identical with those according to cases without residual stresses. Therefore, it is safe to use the same interaction formulae in Eqs. (18)–(21).

Discussion of results

- The flange stiffness affects remarkably the web buckling resistance by resisting the web deformations outside its plane.

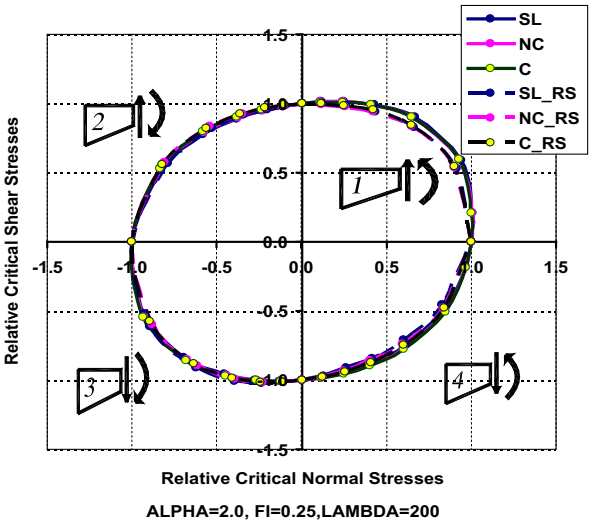

Fig. 26 Comparison between relative interaction with- and without residual stresses ($\alpha = 2.0$, $\phi = 0.25$, $\lambda = 200$).

- A compact flange may increase the bending buckling resistance remarkably [10], but the increase in shear buckling resistance is quite limited.
- Comparing relative interaction results, Fig. 12, for $\alpha = 1$, $\phi = 0.125$, with those for $\alpha = 2.0$, $\phi = 0.25$, Fig. 16, we notice that both plots are almost identical. This indicates the parameter "ϕ/α" as an important one, which is consistent with the results indicated in Mirambell and Zarate [4]. The effect of web slenderness is small, when inspecting relative values related to pure critical bending, or, shear stresses.
- The resistance of the tapered web against buckling is directly proportional to the tapering angle value only in cases, where the moment stresses increase the shear resistance of the tapered web (Loading Types 1 and 3). The increase in moment resistance due to tapering is limited. Nevertheless, the tapering angle increases the shear resistance significantly (up to 20%), This behavior can be graphically explained as given in Fig. 17: The primary horizontal tensile stress "f_M", which is proportional to F_y, remarkably reduces the primary shear stress "q_V", which is proportional to $0.58F_y$.
- Figs. 25 and 26 show that residual stresses do not influence the relative interaction; yet, it remarkably reduces the shear and bending critical stresses.
- Flange slenderness affects clearly the tapered web buckling stresses. A compact flange increases the stresses up to 30% in case of pure moment. However, the slenderness of flanges has no, or little, effect on relative values.

Conclusions and recommendations

The current work presents a geometric and loading FEM model to determine the behavior of plate girder tapered web under interactive combination of shear- and bending stresses. The model provides accurate and homogeneous values of either stress type. The loading is applied to provide either constant shear or moment stress separately. In each investigated

case, the ratio between both stresses is kept the same, and their value is iterated until convergence. This method makes it possible to capture all critical values, especially those beyond 1.0. The critical stresses and corresponding relative values are plotted representing the behavior of tapered web plates under combined moment and shear.

The results are given directly graphically, or, it is easier and safe to apply the direct solution using the proposed approximate formulae. Accurate values of critical stresses could either be taken from the given figures, or directly from (18) and (20).

Assuming that residual stresses are element Loads, the elements of the stiffness matrix change and influence the Eigen-values (critical buckling loads). We notice a remarkable reduction in critical shear and bending stresses. However, almost no influence on relative values is found. Therefore, the same proposed approximate formulae are valid for cases with residual stresses.

It is recommended that future works study the ultimate pure load behavior of such tapered plates.

Conflict of interest

None declared.

References

[1] EN 1993-1-5. Eurocode 3. Design of Steel Structures, Part 1–5. Plated structural Elements, 2006.
[2] AASHTO. LRFD Bridge Design Specifications, Washington, DC, 2009.
[3] A. Eid. Ausbeulen trapezfoermigen Platten, Ph.D., ETH, Zurich, 1957.
[4] E. Mirambell, A.V. Zarate, Ultimate strength of tapered steel plate girders under combined shear and bending moment, Adv. Steel Struct. 2 (2005) 1383–1388.
[5] I. Estrada, E. Real, E. Mirambell, A new developed expression to determine more realistically the shear buckling stress in steel plate structures, J. Construct. Steel Res. 64 (2008) 737–747.
[6] R. Chacon, E. Mirambell, E. Real, Influence of designer-assumed initial conditions on the numerical modeling of steel plate girders subjected to patch loading, Thin-Walled Struct. 47 (2009) 391–402.
[7] E. Mirambell, A.V. Zarate, Web buckling of tapered plate girders, Proc. Inst. Civil Eng. Struct. 140 (2000) 51–60.
[8] E. Mirambell, A.V. Zarate, Shear strength of tapered steel plate girders, Proc. ICE – Struct. Build. 157 (5) (2004) 343–354.
[9] A. Bedynek, E. Real, E. Mirambell, Tapered plate girders under shear: tests and numerical research, Eng. Struct. 46 (2013) 350–358.
[10] M. Abu-Hamd, I. Abu-Hamd. Buckling strength of tapered bridge girders under shear and bending, in: Proceedings of the Structural Stability Research Council, Annual Stability Conference, May 2011.
[11] S.P. Timoshinko, J.M. Gere, Theory of Elastic Stability, McGraw-Hill Book Company, 1936.
[12] C.J. Earls. Observation on Eigenvalue buckling analysis within a finite element context, in: Proceedings of the Structural Stability Research Council, Annual Stability Conference, 2007.
[13] R. Ziemian (Ed.), Guide to Stability Design Criteria for Metal Structures, John Wiley & Sons, 2010.
[14] E. Real, A. Bedynek, E. Mirambell. Numerical and experimental research in tapered steel plate girders subjected to shear, in: E. Batista, et al. (Eds), SDSS'Rio 2010 Stability and Ductility of Steel Structures, 2010, 747–754.
[15] ANSYS, Theory Manual, Swansea Company, 2009.